DESIGN OF A FLEXTENSIONAL PIEZOACTUATOR BASED ON FUNCTIONALLY GRADED MATERIAL CONCEPT USING THE TOPOLOGY OPTIMIZATION METHOD

Ricardo Cesare Roman Amigo, mail@amigoricardo.com
Emilio Carlos Nelli Silva, ecnsilva@usp.br
Department of Mechatronics and Mechanical Systems Engineering, Escola Politecnica - Universidade de Sao Paulo
Av. Professor Mello Moraes, 2231, Sao Paulo, SP, 05508-900, Brazil

Abstract. *Piezoelectric actuators enable precise movements based on the piezoelectric effect, by which some materials transform electric potential into mechanical displacements. Flexible coupling structures are usually attached to the ceramic ends to direct and amplify the displacements to the actuator tip. To improve the piezoactuators performance, the coupling structures can be designed by using Functionally Graded Materials (FGM) concept, which consists of gradual change of the effective material properties and can be manufactured through the Spark Plasma Sintering (SPS) technique. Thus, in this work, a graded flexible coupling structure that maximizes the static displacement in a given direction is obtained by using the Topology Optimization Method (TOM), which combines optimization algorithms and the Finite Element Method (FEM) to distribute material inside a fixed domain. The TOM formulation is based on the Solid Isotropic Material with Penalization (SIMP) material model adapted for the FGM concept and on the Continuous Approximation of Material Distribution (CAMD), which can represent continuous change of design variables along the domain. Bi-dimensional examples are presented and their generated displacements are compared with homogeneous actuators performance.*

Keywords: *Topology Optimization, Functionally Graded Material, Piezoelectric Actuators, Spark Plasma Sintering.*

1. INTRODUCTION

Piezoactuators are based on the capability of electromechanical energy conversion presented by some ceramics. To amplify the ceramics displacements, flexible coupling structures are commonly attached to them. This kind of assembly is known as flextensional piezoactuator and it is employed in a wide range of applications, such as ink jet print head (Hyeon and Asipeu, 2009), compact high-dynamic orientation systems (Villgrattner and Ulbrich, 2011) and airplane-wing deformation control (Tzou and Tseng, 1990).

Regarding gains in reliability and performance, flextensional actuators can be designed considering Functionally Graded Materials (FGMs), which are advanced materials with continuously graded properties due to their spatially graded microstructure. FGMs can be manufactured by using several techniques, among which stands out the Spark Plasma Sintering (SPS), which consists in a powder densification process subjected to pressure and eletromagnetic field, simultaneously. The SPS allows sintering process to occur during a short period and with relatively low temperatures (Feng *et al.*, 2005).

Silva *et al.* (2000) introduced the use of the Topology Optimization Method (TOM) as an useful tool for designing flextensional devices. Subsequently, this approach has been extended to the design of FGM piezoelectric actuators (Carbonari *et al.*, 2010), introducing the concept of integral piezoactuators. In an integral piezoactuators the ceramic-metal interfaces are smoothly graded, eliminating the non-linearities and stress concentrations of bonding layers.

Therefore, seeking to expand the role of FGMs in piezoactuators, this work presents the study of optimal topologies for piezoactuators graded coupling structures. For this, TOM is employed by using the FGM-SIMP material model (Paulino and Silva, 2005) to represent property gradations along the design domain. The design optimization is based on the minimization of mean compliance and on the maximization of the output displacement. Regarding manufacturing, the sintering of Copper-Nickel blends is investigated, by measuring their elastic constants and analysing their microstructure.

This article is organized as follows. A briefing of FEM modelling for piezoelectric media is presented in Section 2. The material model adopted in this work and the design problem with its objective functions are specified in Section 3. The numerical implementation of the design problem is detailed in Section 4. The manufacturing and characterization are detailed in Section 5. Finally, some numerical and manufacturing results are presented in Section 6.

2. PIEZOELECTRIC FINITE ELEMENT

As complex topologies are expected, a general method such as Finite Element Method (FEM) is required to perform structural analysis. With design domains that has its width and height dimensions much larger than its thick, the plane stress hypothesis can be made and, thus, the loads are uniformly applied along the domain thickness. Considering actuators operating in low frequency, the inertia effects can be neglected and the problem is modelled through a linear static

analysis, given by Eq. (1) (Lerch, 1990).

$$\begin{bmatrix} \mathbf{K_{uu}} & \mathbf{K_{u\phi}} \\ \mathbf{K_{\phi u}} & -\mathbf{K_{\phi\phi}} \end{bmatrix} \begin{Bmatrix} \mathbf{U} \\ \mathbf{\Phi} \end{Bmatrix} = \begin{Bmatrix} \mathbf{F} \\ \mathbf{Q} \end{Bmatrix} \tag{1}$$

where $\mathbf{K_{uu}}$ denotes the mechanical stiffness matrix, $\mathbf{K_{u\phi}}$ and $\mathbf{K_{\phi u}}$ the piezoelectric coupling matrices, $\mathbf{K_{\phi\phi}}$ the dielectric matrix, $\mathbf{U}$ the mechanical displacement vector, $\mathbf{\Phi}$ the electric potential vector, $\mathbf{F}$ the mechanical load and $\mathbf{Q}$ the electrical load.

3. TOPOLOGY OPTIMIZATION FORMULATION

3.1 Material Model

The topology optimization method seeks an optimal material distribution inside a fixed domain for given purposes. This is made by defining which points should be solid and which points should be void, assigning pseudo-densities equal to 0 or 1, respectively. However, such problem is ill-posed and the usual way to find a solution is by defining a material model that allows intermediate property values. Although solvable, the relaxed problem produces gray regions, where the presence or absence of material is not clear. To recover the discrete nature of the problem, penalization coefficients are introduced by material models to minimize regions with intermediate densities, as made in the Simple Isotropic Material with Penalization, SIMP (Bendsøe, 1989). Aiming FGM designs, SIMP was extended by Paulino and Silva (2005) resulting in the FGM-SIMP model, which has the capability of representing a domain with property changes along certain direction according to a specified law. In this work, the Young's modulus value is related to the position $\mathbf{x}$ by an exponential law, as stated in Eq. (2).

$$E^H(\mathbf{x}) = E_0 e^{\alpha X + \beta Y} \rho(\mathbf{x})^p \tag{2}$$

where $\mathbf{x}$ denotes the node coordinates, $E^H(\mathbf{x})$ the Young's modulus at $\mathbf{x}$, E_0 denotes the reference Young's modulus, $\rho(\mathbf{x})$ the material density, p the penalization factor and α and β define the property changes along directions X and Y, respectively.

3.2 Design Problem

The design problem of this work is to maximize the output displacement of a flextensional actuator when an electric potential is applied to its electrodes. Figure 1 shows two load cases in the domain considered, where Ω_s denotes the design domain and Ω_p denotes the fixed piezoelectric domain.

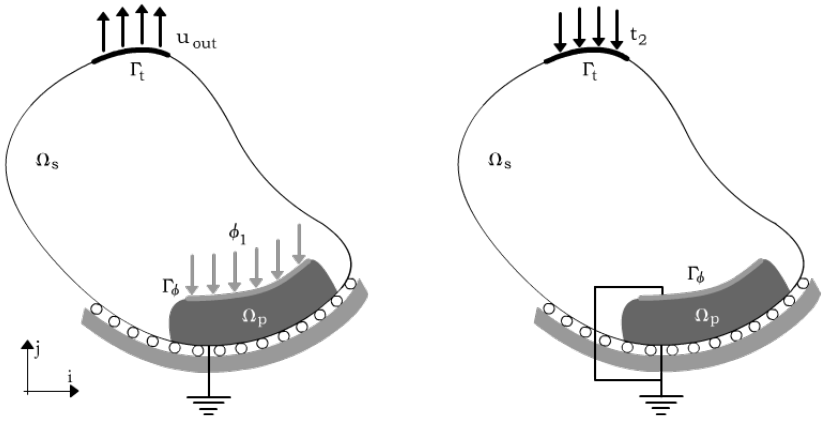

(a) Output displacement; (b) Mean compliance.

Figure 1. Load cases applied to design domain.

The goal of this problem is to achieve the maximum displacement at face Γ_t when an electrical potential ϕ_1 is applied at Γ_ϕ:

$$L_1 = \int_{\Gamma_t} \mathbf{u}_{out}\, d\Gamma \tag{3}$$

where $\mathbf{u}_{out}$ is the output displacement at face Γ_t.

Furthermore, a structural function must be considered to ensure material connection between the output displacement face Γ_t and the piezoceramic, guaranteeing enough stiffness during actuation. Thus, it is necessary to minimize the mean compliance of structure, which is given by Eq. (4).

$$L_2 = \int_{\Gamma_t} \mathbf{t}_2 \cdot \mathbf{u}_2 \, d\Gamma \tag{4}$$

where $\mathbf{t}_2$ denotes a mechanical load, applied to region Γ_t, which generates a displacement $\mathbf{u}_2$. The region Γ_ϕ is kept grounded.

The two objective functions are combined into a single multi-objective function, as shown in Eq. (5).

$$\mathcal{F} = \begin{cases} \frac{L_2}{L_1} & , L_1 \leq 0 \\ \\ w \cdot lnL_1 - (1-w) \cdot lnL_2 & , L_1 > 0 \end{cases} \tag{5}$$

where $w \in [0, 1]$ denotes the weighting coefficient.

Thus, the optimization problem is stated as:

$$\begin{array}{ll} Maximize: & \mathcal{F}(\rho) \\ \rho(\mathbf{x}) & \\ subject\ to: & 0 < \rho \leq 1 \\ & \int_{\Omega_s} \rho d\Omega_s - \Theta_s \leq 0 \end{array} \tag{6}$$

where Ω_s denotes the optimizable region from design domain Ω and Θ_s the upper-bound volume constraint.

4. NUMERICAL IMPLEMENTATION

The implementation software is developed in MATLAB and has its activity diagram shown in Fig. 2.

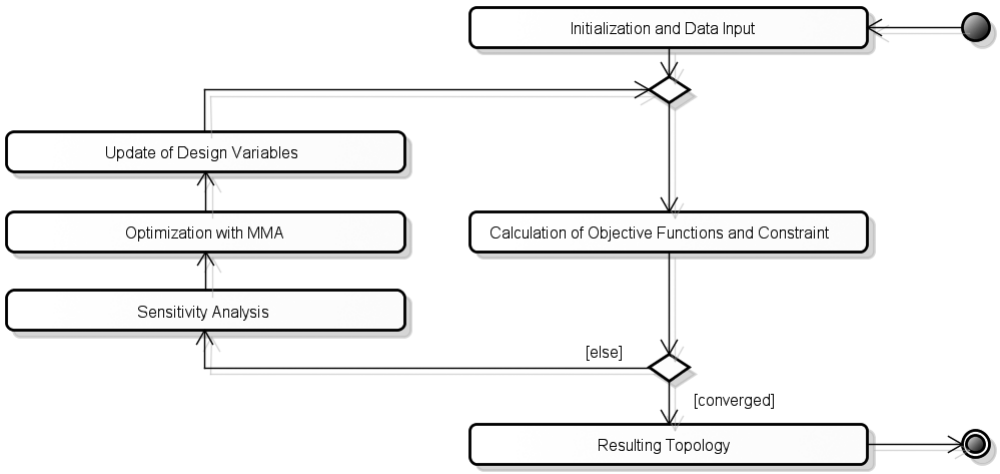

Figure 2. Activity diagram of optimization procedure.

The design domain is meshed using four node bilinear elements considering plane stress hypothesis. The densities defined at each node are interpolated along the domain by the Continuous Approximation of Material Distribution, CAMD (Matsui and Terada, 2004), which uses the shape functions within each element to evaluate its density ρ^e as shown in Eq. (7).

$$\rho^e(\mathbf{x}) = \sum_{i=1}^{4} \rho_i^e N_i^e(\mathbf{x}) \tag{7}$$

where ρ_i^e denotes the nodal density of element e at node i and N_i^e the shape functions of element e related to node i at coordinate $\mathbf{x}$.

Using the MEF approach, the output displacement, stated in Eq. (3), is written as:

$$L_1 = \mathbf{A}^t \cdot \mathbf{U}_1 \tag{8}$$

where $\mathbf{U}_1$ denotes the displacements generated due to the application of an electrical potential at Γ_ϕ and $\mathbf{A}$ denotes a vector consisting of zeros, except at the positions corresponding to the degrees of freedom of the output displacement, where their values are unitary.

The mean compliance stated in Eq. (4), can be written as:

$$L_2 = \mathbf{U}_2^t \cdot \mathbf{K} \cdot \mathbf{U}_2 \tag{9}$$

where $\mathbf{U}_2$ denotes the displacements generated by the application of a compression load at Γ_t and $\mathbf{K}$ denotes the stiffness matrix.

The optimization process uses the Method of Moving Asymptotes, MMA (Svanberg, 1987), to solve the optimization problem. At each iteration, the current densities are informed and then a subproblem is approximated, in which the functions are replaced by convex functions, based mainly on gradient information. The moving asymptotes are updated at each iteration, based on information from previous iteration points.

5. MANUFACTURING

The procedure for manufacturing a FGM piezoactuator is shown in Fig. 3. Initially, a FGM cylinder is sintered using Spark Plasma Sintering (SPS) process, which also has the capability to produce pieces with the desired kind of material gradation, limited by the feasibility of pouring the layers of powder blends as required. Then, this cylinder is machined to obtain a block, which is subjected to Electrical Discharge Machining (EDM) to achieve the designed topology. Lastly, the machined coupling structures are bonded to piezoceramics.

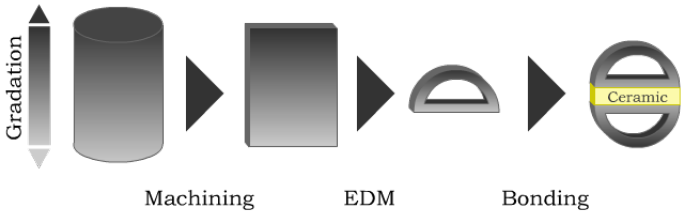

Figure 3. FGM piezoactuator manufacturing procedure.

However, for manufacturing reasons, the gradations must be expressed in terms of mass percentage of each component material, while the property gradation defined by the material model in Eq. (2) is given in terms of Young's modulus. Thus, a Young's modulus curve must be obtained experimentally, by characterizing samples with different mass percentages sintered in SPS machine.

Non-destructive methods for samples characterization, such as by ultrasonic waves, constitute a suitable approach to measure their elastic constants. Adamowski *et al.* (2010) has shown that, having the longitudinal and shear wave velocities inside a material, their elastic constants can be evaluated through some physical relationships. These velocities can be determined from a set of bulk ultrasonic wave phase velocities measured in an arbitrary direction of a sample. This is made, as shown in Fig. 4, by placing the sample between two ultrasound transducers and measuring, with an oscilloscope, the required time for the wave passing through it. When the sample is parallel to transducers, the longitudinal wave propagation prevails and, when the sample is inclined by an angle higher than the critical, the shear wave has preferential propagation.

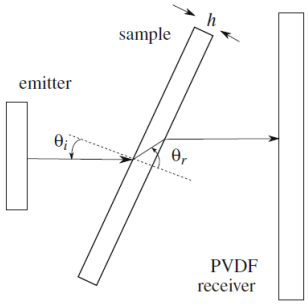

Figure 4. Schematic of goniometer device (Adamowski *et al.*, 2010).

6. RESULTS

6.1 Numerical Results

The results presented in this section are obtained by considering one fourth of a symmetric piezoactuator given by the design domain in Fig. 5 with PZT as piezoceramic and with Copper and/or Nickel as coupling structure. A $10 \times 5\ mm$ domain, with a $7.5 \times 0.5\ mm$ piezoceramic, is discretized in 3200 square elements with $1\ mm$ of thickness. The volume constraint imposed is 25% of the initial design domain volume.

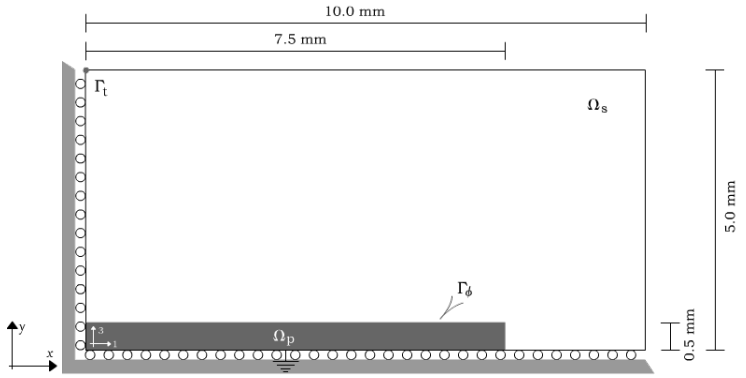

Figure 5. Design domain.

Different material distributions inside the design domain are tested: (i) homogeneous Nickel; (ii) homogeneous Cu; (iii) Copper to Nickel exponential gradation along x; (iv) Nickel to Copper exponential gradation along y. The resulting topologies shown in Fig. 6 are obtained with $w = 0.25$.

Despite similar topologies, the graded domains presented larger static displacements at the output face Γ_t than the homogeneous Nickel domain. The Table 1 presents the output displacements achieved by each case when applying an electric potential of $-100V$ to the Γ_ϕ electrode.

Table 1. Output displacements for post-processed structures for each gradation case.

	Output displacement (nm)
Homogeneous Ni	358
Homogeneous Cu	401
Cu-Ni along x	430
Ni-Cu along y	435

6.2 Manufacturing Results

To manufacture prototypes of numerical results, it is necessary to know the mixture of materials that gives each property value of the domain gradation. Thus, five homogeneous samples with different proportions of Cooper and Nickel are sintered to map the relations between Young's modulus and mass percentage. The samples, with Cu-Ni percentages of $0-100$, $25-75$, $50-50$, $75-25$ and $100-0$, are manufactured in a SPS machine with the same sintering routine, given by heating rate of $100\ ^oC/min$ with a $2\ min$ holding time at $800\ ^oC$.

The characterization of the Cu-Ni samples is made by using a goniometer device immersed in distilled water. The emitter is a focused transducer with center frequency of 5 MHz and diameter of 10 mm and the receiver is a diffraction-free PVDF transducer. In Table 2, the longitudinal wave velocity is measured with the sample parallel to transducers and the shear wave velocity is measured with the sample inclined by 25 degrees.

Table 2. Wave velocities inside Cu-Ni samples.

Percentage of Cu (in mass)	Longitudinal wave (m/s)	Shear wave (m/s)
0	5530.73	2962.30
25	5423.87	2754.00
50	5142.71	2605.58
75	3884.55	2812.62
100	3820.70	1973.11

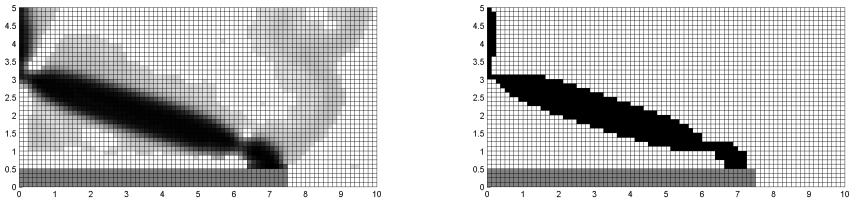

(a) Homogeneous Ni;

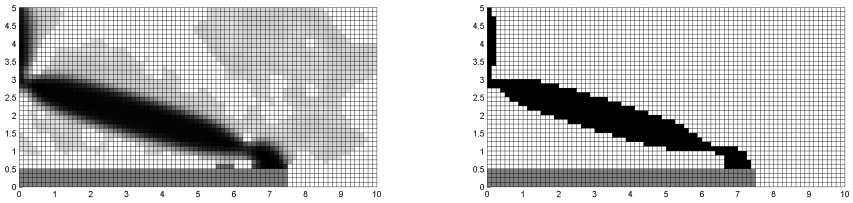

(b) Homogeneous Cu;

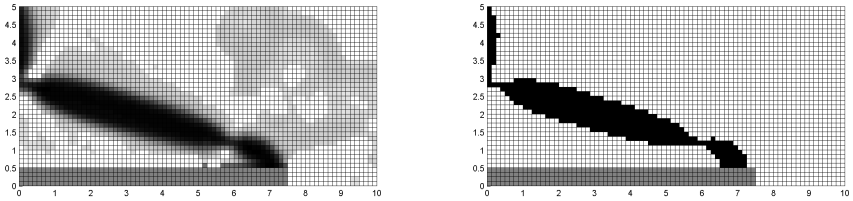

(c) Cu-Ni along x;

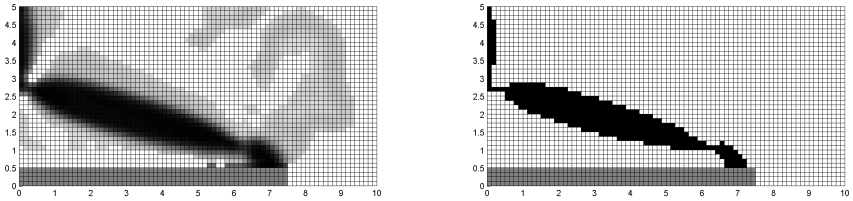

(d) Ni-Cu along y.

Figure 6. Resulting topologies and post-processed structures.

Based on measured wave velocities, the elastic constants are evaluated. The full-nickel sample presented $271.65\,GPa$ as P-wave modulus and 0.2989 as Poisson ratio, resulting in a Young's modulus of $202.44\,GPa$, near to the expected. However, the full-copper sample presented $138.62GPa$ as P-wave modulus and 0.3182 as Poisson ratio, resulting in a Young's modulus of $97.46\,GPa$, much lower than expected - around $130GPa$. Figure 7 shows the interpolated curve of P-wave modulus by the fraction of each material.

Aiming to investigate the reasons for the discrepant wave velocities presented by samples with higher Cu percentage, the metallography of the full-copper sample is performed. Figure 8 shows a region where lots of black islands can be seen. These islands may appear due to carbon diffusion from the graphite die, used in SPS process, to the sample. Quantitative color spectrum analysis with images acquired from the sample surface gives Carbon concentration around 6.0% in terms of area, which can be estimated by 1.52% in terms of mass (Cardarelli, 2000). In the Carbon-Copper phase diagram (ASM, 1992) can be seen that Carbon has relatively low solubility in Copper (0.01% in weight percent of Carbon). This fact causes graphite accumulation nearby to grain contours and makes the material more ductile. In the Carbon-Nickel phase diagram, the solubility observed is much higher, being 0.60% in weight percent of Carbon, extendible to 1.60% at $1314\,^oC$.

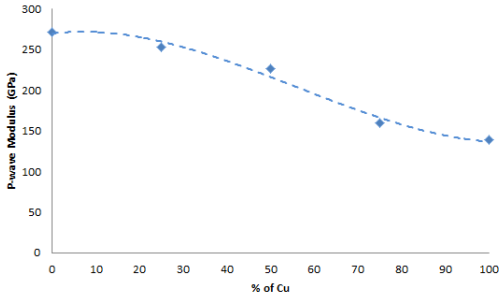

Figure 7. P-wave modulus along Cu-Ni gradation.

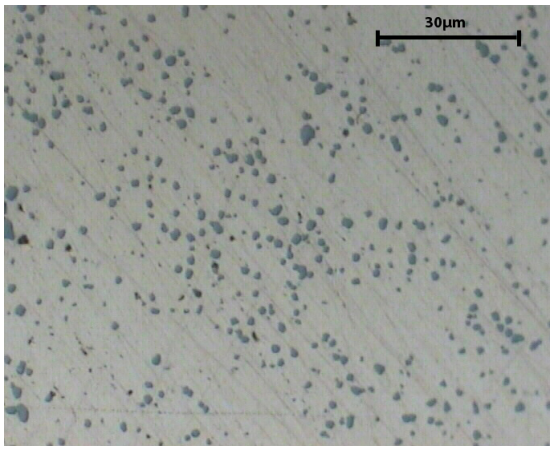

Figure 8. Copper Sample

7. CONCLUSION

The numerical results obtained by this work show that the use of FGMs leads to performance gains in the design of flextensional piezoactuators. For the studied cases, the static displacements achieved with graded coupling structures are larger than with homogeneous coupling structures. Depending on the gradation law, the use of graded structures may imply in output displacements 8.40% larger than homogeneous structures.

The characterization of Cu-Ni samples highlights problems in copper sintering using SPS with graphite dies. To avoid it, some working options are: (i) to submit the sintered pieces to some annealing process to extract carbon particles; (ii) not to use gradations with high copper percentage or not to use copper among the design materials; (iii) to use dies made with another material besides graphite.

8. ACKNOWLEDGEMENTS

The first author acknowledges the financial support of CNPq (National Council for Research and Development) under grant 558411/2010-0 and Prof. Dr. Izabel Fernanda Machado, Dr. Marco Aurelio Brizotti Andrade and Dr. Nicolas Perez at Escola Politecnica, University of Sao Paulo, for their collaboration in the experimental characterizations. The second author acknowledges the financial support of CNPq under grant 303689/2009-9. The authors are also grateful to Dr. Krister Svanberg for having supplied the MMA-code.

9. REFERENCES

Adamowski, J.C., Buiochi, F. and Higuti, R.T., 2010. "Ultrasonic material characterization using large-aperture pvdf receivers". *Ultrasonics*, Vol. 50, pp. 110–115.

ASM, 1992. *ASM Metals Handbook - Alloy Phase Diagrams (Vol. 3)*.

Bendsøe, M.P., 1989. "Optimal shape design as a material distribution problem". *Structural Optimization*, Vol. 1, pp. 193–202.

Carbonari, R.C., Paulino, G.H. and Silva, E.C.N., 2010. "Integral piezoactuator system with optimum placement of functionally graded material: a topology optimization paradigm". *Journal of Intelligent Material Systems and Structures*, Vol. 21, pp. 1653–1668.

Cardarelli, F., 2000. *Materials Handbook: A Concise Desktop Reference*. Springer.

Feng, H., Meng, Q., Zhou, Y. and Jia, D., 2005. "Spark plasma sintering of functionally graded material in the ti-tib2-b system". *Materials Science and Engineering*, Vol. A397, pp. 92–97.

Hyeon, C.G. and Asipeu, A.R.M., 2009. "Hybrid type ink jet print head, has ink chamber for storing ink, ben position extended to ink chamber, piezoactuator installed in bottom surface of ink chamber and nozzle formed in chamber bottom". Technical report, Patent Number: KR2010128953-A.

Lerch, R., 1990. "Simulation of piezoelectric devices by two-and-three-dimensional finites elements". *IEEE Transaction on Ultrasonics, Ferroelectrics and Frequency Control*, Vol. 37,2, pp. 233–247.

Matsui, K. and Terada, K., 2004. "Continuous approximation for material distribution for topology optimization". *International Journal for Numerical Methods in Engineering*, Vol. 59, pp. 1925–1944.

Paulino, G.H. and Silva, E.C.N., 2005. "Design of functionally graded structures using topology optimization". *Material Science Forum*, Vol. 492-493, pp. 435–440.

Silva, E.C.N., Nishiwaki, S. and Kikuchi, N., 2000. "Topology optimization design of flextensional actuators". *IEEE Transaction on Ultrasonics, Ferroelectrics and Frequency Control*, Vol. 47,3, pp. 657–671.

Svanberg, K., 1987. "The method of moving asymptotes - a new method for structural optimization". *International Journal for Numerical Methods in Engineering*, Vol. 24, pp. 359–373.

Tzou, H.S. and Tseng, C.I., 1990. "Distributed piezoelectric sensor actuator design for dynamic measurement control of distributed parameter-systems: a piezoelectric finite-element approach". *Journal of Sound and Vibration*, Vol. 138, pp. 17–34.

Villgrattner, T. and Ulbrich, H., 2011. "Design and control of a compact high-dynamic camera-orientarion system". *IEEE/ASME Transactions on Mechatronics*, Vol. 16,2, pp. 221–231.

10. RESPONSIBILITY NOTICE

The authors are the only responsible for the printed material included in this paper